# COMMUNICATIONS

[10] "Producing coated particles by grinding in the presence of reactive species: "M. R. Linford, US-A 6,132,801 **2000**.

[11] S. Xu, G. Liu, *Langmuir* **1997**, *13*, 127–129.

[12] N. L. Abbott, J. P. Folkers, G. M. Whitesides, *Science* **1992**, *257*, 1380–1382.

[13] P. S. Cremer, J. T. Groves, L. A. Kung, S. G. Boxer, *Langmuir* **1999**, *15*, 3893–3896.

[14] C. D. Bain, E. B. Troughton, Y.-T. Tao, J. Evall, G. M. Whitesides, R. G. Nuzzo, *J. Am. Chem. Soc.* **1989**, *111*, 321–335.

[15] A. Ulman, *An Introduction to Ultrathin Organic Films from Langmuir–Blodgett to Self-Assembly*, Academic Press, Boston **1991**.

[16] C. D. Bain, G. M. Whitesides, *J. Phys. Chem.* **1989**, *93*, 1670–1673.

[17] P. E. Laibinis, R. G. Nuzzo, G. M. Whitesides, *J. Phys. Chem.* **1992**, *96*, 5097–5105.

## Synthesis of Very Thin 1D and 2D CdWO$_4$ Nanoparticles with Improved Fluorescence Behavior by Polymer-Controlled Crystallization**

Shu-Hong Yu,* Markus Antonietti, Helmut Cölfen, and Michael Giersig

Nanosized building blocks with lower dimensionality, such as nanotubes, nanowires, nanorods, and ultrathin nanoplatelets have recently experienced a heightened interest.[1–9] These systems with at least one restricted dimension offer opportunities for investigating the influence of size and dimensionality on optical, magnetic, and electronic properties.[2] They can also be used as one component for a nanocomposite material to significantly improve the material properties.[8] Recent efforts have focused on the development of new synthetic routes for preparing nanorods, nanowires, or nanotubes with uniform sizes and aspect ratios, for example, nanorods/nanowires of BaCrO$_4$,[3] CdSe,[4] metal nanorods: Cu,[5a] Fe,[5b] Ag,[5c,d] Au,[6] FeOOH,[7] and vanadium oxide nanotubes (VO$_x$-NTs).[9] A family of long semiconductor-oxide nanobelts with widths of 30 to 300 nanometers and width-to-thickness ratios of 5 to 10 was successfully synthesized by simply evaporating the desired commercial metal–oxide powders at high temperature.[2b] The formation of a 2D

[*] Dr. S.-H. Yu, Prof. Dr. M. Antonietti, Dr. H. Cölfen
Max Planck Institute of Colloids and Interfaces
Department of Colloid Chemistry
MPI Research Campus Golm, 14424 Potsdam (Germany)
Fax: (+49) 331-567-9502
E-mail: shyu@mpikg-golm.mpg.de
Dr. M. Giersig
Hahn-Meitner-Institut, Abt. Physikalische Chemie
Glienickerstrasse 100, 15109 Berlin (Germany)

Supporting information for this article is available on the WWW under http://www.angewandte.org or from the author.

BaCrO$_4$ nanorod monolayer assembly using the Langmuir–Blodgett technique was also reported,[10] and 2D wurtzite ZnS nanosheets were fabricated by a solution-based template method.[11]

Recently, tungstate materials have attracted much interest because of their luminescence behavior, structural properties, and potential applications.[12] Cadmium tungstate (CdWO$_4$) nanocrystals with a monoclinic wolframite structure are interesting because of their high average refractive index, low radiation damage, low afterglow, and high X-ray absorption coefficient;[13] they can be used, for instance, as an X-ray scintillator.[14, 15] Other tungstates with Scheelite structure MWO$_4$ (M = Ca, Ba, Pb) also display interesting excitonic luminescence, thermoluminescence, and stimulated Raman scattering (SRS) behavior.

To date, the procedure regarded as optimal to prepare CdWO$_4$ nanorods is a hydrothermal process at 130 °C.[16] The nanorods of different compositions reported so far generally have rather small aspect ratios (length-to-diameter) of 2–10,[17] which results in weak symmetry-breaking surface effects. In addition a reverse micelle templating method has recently been used to synthesize uniform BaWO$_4$ nanorods with diameters of 5 nm and aspect ratios of about 150 by using barium bis(2-ethylhexyl)sulfosuccinate [Ba(AOT)$_2$] micelles, which are treated with NaAOT microemulsion droplets containing sodium tungstate (Na$_2$WO$_4$).[17] The large excess of surfactants as well as the very low concentration throughout synthesis, however, could restrict the applicability of this procedure.

Herein, we present a facile aqueous-solution route for the synthesis of extremely thin 1D and 2D CdWO$_4$ nanoparticles with controlled sizes (length, width, thickness) by using a combination of the double-jet injection of simple inorganic reactants and double-hydrophilic block copolymers (DHBCs) as crystal-growth modifiers.

DHBCs have been introduced as very efficient inhibitors and crystal-growth modifiers[18] and have already shown their potential for the morphosynthesis of calcium carbonate, barium sulfate, calcium phosphates, and zinc oxide crystals.[19] To differentiate between the influence of process parameters and the chemical influence of the DHBCs, CdWO$_4$ was crystallized in a set of experiments in the absence of polymer. The X-ray diffraction (XRD) pattern in Figure 1a demonstrates that well-crystallized CdWO$_4$ particles can be easily synthesized at room temperature, which can be indexed as monoclinic wolframite structure with unit cell parameters $a = 5.029$, $b = 5.859$, $c = 5.074$ Å (JSPDS Card: 14-676). The sharper nature of the diffraction peaks 100, 200, and 002 suggests possible preferential orientation along these directions. In addition, the 010 diffraction peak is very weak and broadened, which indicates that the thickness direction will be along the $b$ axis, which was confirmed by high-resolution (HR) TEM results.

The corresponding TEM image in Figure 2a shows very thin, uniform CdWO$_4$ nanorods/nanobelts with lengths in the range of 1–2 μm and a uniform width of 70 nm along their entire length (aspect ratio of about 30). No different contrast was observed, which suggests the perfect growth of the nanoparticles and uniform thickness. Large scale, lower-
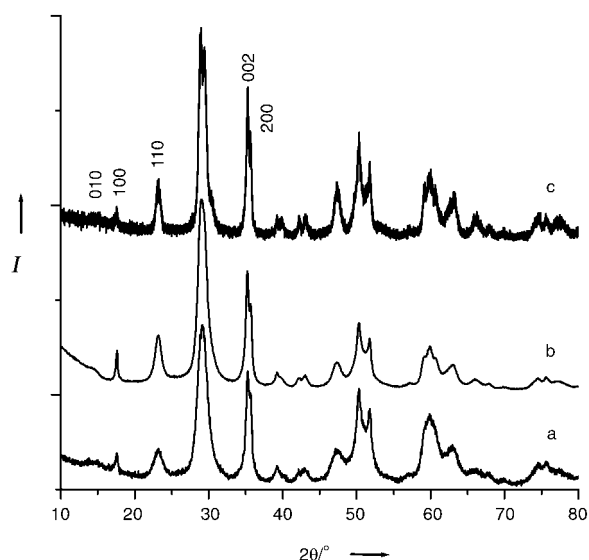
Figure 1. X-ray diffraction patterns of the CdWO$_4$ samples obtained under different conditions: a) initial solution: 20 mL, pH 5.3, double jet, end solution: $[Cd^{2+}]/[WO_4^{2-}] = 8.3 \times 10^{-3}$ M, at room temperature; b) and c) pH 5.3, double jet, end solution $[Cd^{2+}]/[WO_4^{2-}] = 8.3 \times 10^{-3}$ M, then hydrothermal crystallization: b) 80 °C, 6 h; c) 120 °C, 6 h.
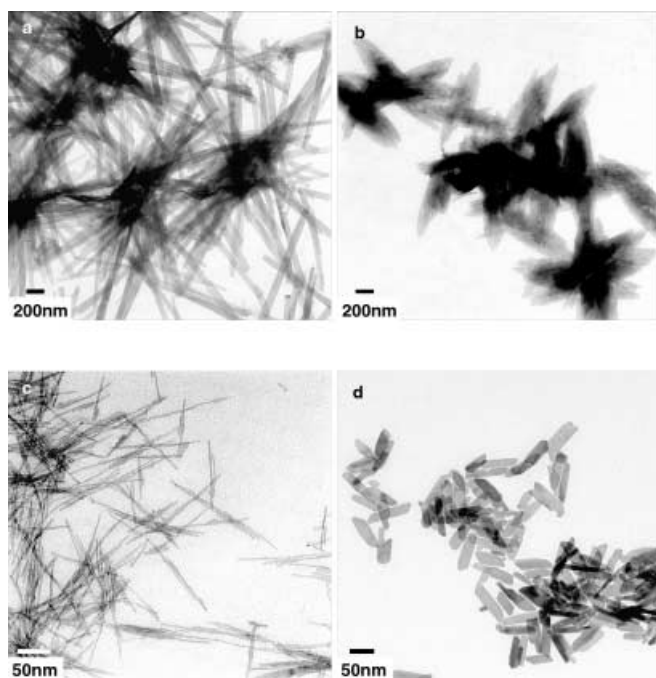


Figure 2. TEM images of the samples obtained under different conditions: a) and b) no additives: a) pH 5.3, double jet, $[Cd^{2+}]/[WO_4^{2-}] = 8.3 \times 10^{-3}$ M (end solution), at room temperature, b) pH 5.3, double jet, $[Cd^{2+}]/[WO_4^{2-}] = 8.3 \times 10^{-3}$ M (end solution), then hydrothermal crystallization: 80 °C, 6 h, c) pH 5.3, in the presence of PEG-*b*-PMAA(1 g L$^{-1}$), 20 mL, double jet, $[Cd^{2+}]/[WO_4^{2-}] = 8.3 \times 10^{-3}$ M (end solution), then hydrothermal crystallization: 80 °C, 6 h, d) direct hydrothermal treatment of 20 mL solution containing equal molar $[Cd^{2+}]/[WO_4^{2-}] = 8.3 \times 10^{-2}$ M, pH 5.3, at 130 °C, 6 h, in the presence of 1 g L$^{-1}$ PEG-*b*-PMAA-PO$_3$H$_2$ (21 %).

magnification TEM images also show that all the longer nanorods/nanobelts tend to aggregate towards nested, starlike clusters (see Supporting Information Figure 1 a and Figure 1 b). Successive hydrothermal ripening after the dou-

ble-jet reaction leads to a rearrangement of the rods into 2D lens-shaped, raftlike superstructures (Figure 2 b) with a resulting lower aspect ratio. The thickness of the rods and the raftlike superstructures was shown to be 6–7 nm by scanning force microscopy (SFM) topography height profiles (see Supporting Information Figures 2 a,b). The structure modeling data clearly shows the W octahedra chain within the wolframite structure. The thin nature of the elongated nanoparticles could be related with the chain structure of the W octahedra in the wolframite type structure.[20] (see Supporting Information Figure 3).

An optional hydrothermal ripening of the CdWO$_4$ nanorods at different temperatures leads either to further self-assembly into 2D raftlike structures (Figure 2 b and Supporting Information Figure 1 d) or the formation of 2D single-crystalline nanoplatelets (Figure 2 d). The self-organization of the nanorods into 2D structures induced by hydrothermal treatment is very similar to that reported for BaWO$_4$ and BaCrO$_4$ nanorods,[10] but differs significantly from the assembly of the short BaCrO$_4$ and CdSe nanorods where ribbonlike and vertical rectangular/hexagonal superstructures are favored.[3a, 4]

There are two reasons for the rods to align parallel,[17] first, to maximize the entropy of the self-assembled structure of rodlike or nematic objects by minimizing the excluded volume per particle in the array, as first suggested by Onsager,[21] and second, because of the higher sum of van der Waals forces along the length of a nanorod as compared to its tip.[6]

The aspect ratio in absence of the polymer is already about 30, which is higher than the previously reported values for BaCrO$_4$ and CdSe.[3a, 4] Additionally, these particles are comparably thin, which is important for the mechanical performance in nanocomposites.[8]

In a second step, the DHBC poly(ethylene glycol)-*block*-poly(methacrylic acid) (PEG-*b*-PMAA) was added to the solvent reservoir before the double-jet crystallization process and the mixture was then hydrothermally ripened at 80 °C. Figure 2 c shows that in this case, uniform nanofibers with a diameter of 2.5 nm, a length of 100–210 nm, and an aspect ratio of 40–85 can be readily obtained. These nanofibers can now be regarded as "real" 1D objects, since the number of surface atoms is comparable with those embedded within the structure. In addition, it is seen that the single fibers are well separated, which indicates a sufficient steric stabilization brought about by the adsorbed DHBCs. Hydrothermal ripening at 80 °C for longer time or at higher temperatures (120 °C) results in this case again in a co-alignment of the rods along their axis to form similar raftlike and very thin 2D-superstructures, as described above (see Supporting Information Figures 1 c and d).

In addition, a new polymer-driven morphology arises when the partly phosphonated hydrophilic block copolymer PEG-*b*-PMAA-PO$_3$H$_2$ (21 %; 1 g L$^{-1}$) is added at an elevated temperature of 130 °C even without using the double-jets but at higher concentrations ($8.3 \times 10^{-2}$ M) and coupled supersaturation. Figure 2 d shows that very thin platelike particles with a width of 17–28 nm, a length of 55–110 nm, and an aspect ratio of 2–4 are obtained by a direct hydrothermal process.

The HRTEM magnification in Figure 3a shows that the particles obtained in the absence of polymer are very thin, as seen by a tilted structure (indicated by the arrow). The nanobelts show the preferential orientation growth in length
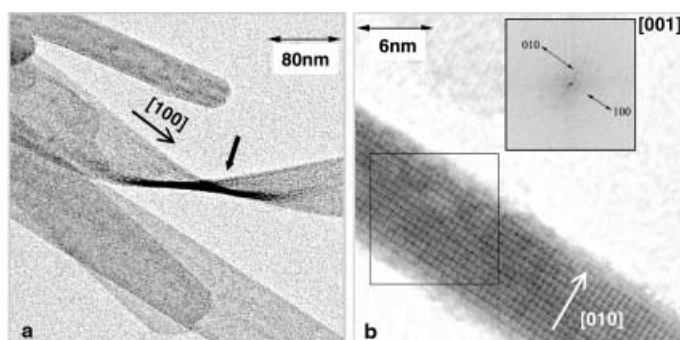


Figure 3. TEM and HRTEM images of the samples obtained under different conditions: a) No additives: pH 5.3, double jet, final solution $[Cd^{2+}]/[WO_4^{2-}] = 8.3 \times 10^{-3}$ M, at room temperature, showing the very thin nanobelts (indicated by the arrow), b) HRTEM image taken along [001], shows the clear lattice fringes of [100] and [010] with spacing 5.86 Å and 5.02 Å, respectively. The thickness of the short sheetlike nanoplates is about 8 nm.
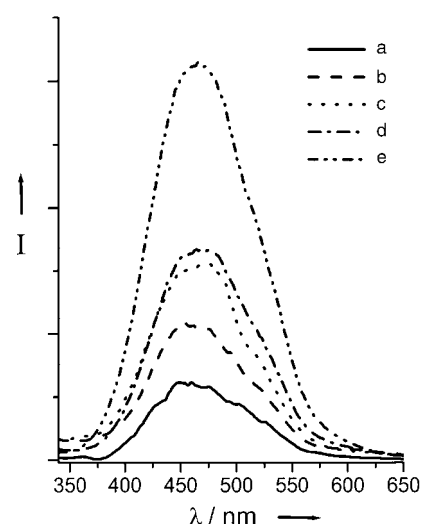


Figure 4. Room temperature photoluminescence spectra of the samples obtained under different conditions: a) pH 5.26, double jet, final solution $[Cd^{2+}]/[WO_4^{2-}] = 8.3 \times 10^{-3}$ M; b) and c) pH 5.26, double jet, final solution $[Cd^{2+}]/[WO_4^{2-}] = 8.3 \times 10^{-3}$ M, then hydrothermal crystallization: b) 80 °C, 6 h; c) 120 °C, 6 h; d) pH 5.3, in the presence of PEG-b-PMAA (1 g L$^{-1}$), 20 mL, double jet, final solution $[Cd^{2+}]/[WO_4^{2-}] = 8.3 \times 10^{-3}$ M, then hydrothermal crystallization: 80 °C, 6 h. e) direct hydrothermal treatment of 20 mL solution containing equal molar $[Cd^{2+}]/[WO_4^{2-}] = 8.3 \times 10^{-4}$ M, pH 5.3, at 130 °C, 6 h, in the presence of 1 g L$^{-1}$ PEG-b-PMAA-PO$_3$H$_2$ (21 %).

along the *a* axis and width along the *c* axis (see Supporting Information Figure 2c). The HRTEM image in Figure 3b was taken exactly along the axis [001] of the nanoplatelets, showing clearly the lattice fringes of the [100] and [010] planes. The short sheetlike nanoplatelets with thickness of about 8 nm preferentially grew along [100] and [001]. That the crystals along the *b* axis are thin and much more elongated along the *c* and *a* axes is again consistent with the above XRD results.

The slow and controlled reactant addition by the double-jet technique under stirring maintains formation of intermediate amorphous nanoparticles at the jets[18b] so that nanoparticles are the precursors for further particle growth rather than ionic species, an important difference to previous reports.[16] This growth mechanism is crucial to obtain the observed nanobelt structure (Figure 2a and Figure 3a). In contrast, the direct mixing of reactants at room temperature under stirring without using the double-jet technique can only produce large aggregates composed of very poorly defined thin platelike particles (data not shown).

Atomic modeling of the exposed crystal surfaces can indicate the structure specificity. The surface structure cleavage of the CdWO$_4$ crystals (Supporting Information Figure 4) shows that the (100) face contains W octahedral anions in a zigzag orientation, which shows that this face will not be favorable for the adsorption of the negatively charged polymer groups, and leads to the detected fastest growth rate along the [100] direction. A view along the *b* axis reveals a regular linear alignment of the tungstate clusters and consequently of the Cd$^{2+}$ ions in a favorable orientation for polymer adsorption on the (010) face.

Figure 4 shows the luminescence spectra of the different CdWO$_4$ nanostructures obtained under different conditions

and with different polymers, but similar concentrations. The spectral characteristics were very similar to those of the other scheelite tungstate crystals (AWO$_4$, A = Pb, Ca, Ba, Sr).[22] The absolute luminescence intensity increases with increasing hydrothermal crystallization temperature (Figure 4a–c), and is an indication of the perfection of the crystals. Quite unexpectedly, the luminescence efficiency is further increased in the presence of the different DHBCs (at lower crystallization temperature), where the best-performing system increases in efficiency by a factor of two. This increase is explained by a highly perfected structure where quenching surface defects are suppressed or blocked by the polymers. The increase of luminescence efficiency by blocking of surface states was observed for DHBC-stabilized CdS quantum dots,[23] and perfecting crystal surfaces by surface-active polymers was described very recently.[24]

The CdWO$_4$ nanostructures obtained in the absence of polymer exhibit a blue emission band in the range 400–550 nm centered around 460 nm when excited at 253 nm, which agrees well with the data for the single crystals obtained at high temperatures,[14] but is blue-shifted compared to the reported "intrinsic luminescence" at 480–490 nm.[25] The blue-emission structure of all three samples contains at least two or three components. Generally, the presence of Gaussian components indicates that the electronic levels corresponding to relaxed excited states of an emission center belong to a degenerated excited states influenced by some perturbation.[26] The emission-band shape might be explained considering Jahn–Teller active vibrational modes of $t_2$ symmetry which influence the WO$_4^{2-}$ complex anion of slightly distorted tetrahedral symmetry to lead to a structured absorption band for the A$_1 \rightarrow$ T$_{1(2)}$ transitions.[26, 27] The decomposition of the

band into individual components results in three Gaussians with their maximum located at 423, 451, and 483 nm, respectively, to give good agreement with the experimental data.[28] The subsequent hydrothermal treatment leads to the red-shift of the three components (Supporting Information: Figures 5 a,c and Table 1).

Similarly, the deconvolution of the emission spectra of the two samples made in the presence of DHBCs reveal an additional green component at 501 nm or 509 nm, respectively (see Supporting Information Figures 5 d,e and Table 1). The comparable amount of the blue and green emission components can be used, taking advantage of the fact that all the recombination processes are transferred to the green component by an efficient energy transfer through free charge carriers.[29] Thus the remaining blue emission component is almost free of recombination processes. The decomposition of the band is not unique since the individual Gaussian components strongly overlap which makes the numerical solution rather unstable. The correlation of energy transfer processes in the blue and green emission components in the synthesized particular systems with lower dimensionality deserves further investigation in time and temperature resolved experiments.

In summary, we have found a simple aqueous route to prepare uniform and very thin $CdWO_4$ nanorods/nanobelts and elongated nanosheets at room temperature starting from simple inorganic reactants by the double-jet crystallization technique. This technique provides nanoparticulate precursors for further crystallization which is in contrast to previously reported techniques. Additionally, application of two different double-hydrophilic block copolymers throughout a hydrothermal ripening process allowed a fine tuning of both crystal morphology and crystal superstructure, for example, 2D raftlike structures could be formed by a hydrothermal ripening process. The prepared structures display a very strong blue/green luminescence at room temperature, where the quantum efficiency is highly improved by addition of the DHBCs. This effect is speculatively attributed to a perfecting of the nanocrystals and/or blocking of quenching surface states by the DHBCs. This approach is expected to form a new general route for the controlled morphosynthesis of tungstate luminescence materials in restricted dimensions, with controllable size and shape, the solid-state optical properties of which are of interest.

## Experimental Section

All chemicals were obtained from Aldrich and were used without further purification. A commercial block copolymer PEG-*b*-PMAA (PEG = 3000 g mol$^{-1}$, PMAA = 700 g mol$^{-1}$) was obtained from Th. Goldschmidt AG, Essen, Germany. The carboxylic acid groups of this copolymer were partially phosphonated (21 %) to give a copolymer with carboxyl and phosphonated groups, PEG-*b*-PMAA-PO$_3$H$_2$, according to ref. [18b].

The precipitation of $CdWO_4$ was carried out in a double-jet reactor thermostated at 25 °C as described previously.[18c] A solution of distilled water (20 mL) was adjusted to the desired pH 5.3, by using 1M NaOH or HCl, before it was used for the precipitation of $CdWO_4$. Under vigorous stirring, 0.1M $CdCl_2$ and 0.1M $Na_2WO_4$ were injected through capillaries into a Teflon reaction vessel with a reactant supply of 1 mL h$^{-1}$ for 2 h, which gave a $CdWO_4$ formation rate of $1.39 \times 10^{-4}$ M min$^{-1}$. The reactant supply was stopped after injection for 2 h, and the precipitate was left under

continuous stirring in its mother solution for at least 6 h to ensure complete equilibration. For direct hydrothermal treatment, equal molar $CdCl_2$ and $Na_2WO_4$ ($1.67 \times 10^{-3}$ mol) were mixed in block copolymer solution (20 mL, 1 g L$^{-1}$) under stirring and then the pH value was adjusted to 5.3 by using 1M HCl.

The above solution was poured into a commercial stainless Teflon-lined autoclave of 40 mL capacity (SANPLATEC Company, Japan) after double-jet reaction. The autoclave was maintained at a certain temperature (80–130 °C) for 6 h, and then air cooled to room temperature. The precipitates were collected and washed with distilled water and dried in air for further characterization.

TEM images were taken with a Zeiss EM 912 Omega microscope. HR-TEM was carried out on a Philips CM 12 microscope operating at 120 kV (equipped with an EDAX 9800 analyzer). Dry powder samples were used for the measurements of X-ray powder diffraction (XRD) using a PDS 120 (Nonius GmbH, Solingen) with Cu$_{K\alpha}$ radiation. The photoluminescence (PL) measurements were performed on a Perkin Elmer Luminescence Spectrometer LS50B at room temperature. Scanning force micrographs (SFM) were obtained from a Digital Instruments Nanoscope III in tapping mode (Digital Instruments Inc., Santa Barbara, (CA)). The height profiles of the nanostructures along the solid line were processed by using the Nanoscope software. The samples were prepared by dropping the nanoparticle dispersion onto a freshly cleaved mica substrate. The computer modeling was done with the Cerius$^2$ software (Accelrys).

[1] C. M. Lieber, *Solid State Commun.* **1998**, *107*, 607.

[2] a) J. T. Hu, T. W. Odom, C. M. Lieber, *Acc. Chem. Res.* **1999**, *32*, 435; A. M. Morales, C. M. Lieber, *Science* **1998**, *279*, 208; b) Z. W. Pan, Z. R. Dai, Z. L. Wang, *Science* **2001**, *291*, 1947.

[3] a) M. Li, H. Schnablegger, S. Mann, *Nature* **1999**, *402*, 393; b) S. H. Yu, H. Cölfen, M. Antonietti, *Chem. Eur. J.* **2002**, *8*, in press.

[4] X. G. Peng, L. Manna, W. D. Yang, J. Wickham, E. Scher, A. Kadavanich, A. P. Alivisatos, *Nature* **2000**, *404*, 59.

[5] a) J. Tanori, M. P. Pileni, *Adv. Mater.* **1995**, *7*, 862; b) S.-J. Park, S. Kim, S. Lee, Z. G. Khim, K. Char, T. Hyeon, *J. Am. Chem. Soc.* **2000**, *122*, 8581; c) B. A. Korgel, D. Fitzmaurice, *Adv. Mater.* **1998**, *10*, 661; d) Y. Zhou, S. H. Yu, C. Y. Wang, X. G. Li, Y. R. Zhu, Z. Y. Chen, *Adv. Mater.* **1999**, *11*, 850.

[6] B. Nikoobakht, Z. L. Wang, M. A. El-Sayed, *J. Phys. Chem. B* **2000**, *104*, 8635.

[7] H. Maeda, Y. Maeda, *Langmuir* **1996**, *12*, 1446.

[8] E. P. Giannelis, *Adv. Mater.* **1996**, *8*, 29.

[9] M. E. Spahr, P. Bitterli, R. Nesper, M. Müller, F. Krumeich, H.-U. Nissen, *Angew. Chem.* **1998**, *110*, 1339; *Angew. Chem. Int. Ed.* **1998**, *37*, 1263.

[10] F. Kim, S. Kwan, J. Akana, P. D. Yang, *J. Am. Chem. Soc.* **2001**, *123*, 4360.

[11] S. H. Yu, M. Yoshimura, *Adv. Mater.* **2002**, *14*, 296.

[12] N. Saito, N. Sonoyama, T. Sakata, *Bull. Chem. Soc. Jpn.* **1996**, *69*, 2191.

[13] H. Lotem, Z. Burshtein, *Opt. Lett.* **1987**, *12*, 561.

[14] V. A. Pustovarov, A. L. Krymov, B. Shulgin, *Rev. Sci. Instrum.* **1992**, *63*, 3521.

[15] K. Tanaka, T. Miyajima, N. Shirai, Q. Zhang, R. Nakata, *J. Appl. Phys.* **1995**, *77*, 6581.

[16] H. Liao, Y. Wang, X. Liu, Y. Li, Y. Qian, *Chem. Mater.* **2000**, *12*, 2819.

[17] S. Kwan, F. Kim, J. Akana, P. D. Yang, *Chem. Commun.* **2001**, 447.

[18] a) H. Cölfen, *Macromol. Rapid Commun.* **2001**, *22*, 219, and references therein; b) H. Cölfen, M. Antonietti, *Langmuir* **1998**, *14*, 582; c) M. Sedlak, M. Antonietti, H. Cölfen, *Macromol. Chem. Phys.* **1998**, *199*, 247.

[19] a) M. Antonietti, M. Breulmann, C. Göltner, H. Cölfen, K. K. Wong, D. Walsh, S. Mann, *Chem. Eur. J.* **1998**, *4*, 2493; b) L. Qi, H. Cölfen, M. Antonietti, *Angew. Chem.* **2000**, *112*, 617; *Angew. Chem. Int. Ed.* **2000**, *39*, 604; c) L. Qi, H. Cölfen, M. Antonietti, M. Lei, J. D. Hopwood, A. J. Ashley, S. Mann, *Chem. Eur. J.* **2001**, *7*, 3526; d) M. Öner, J. Norwig, W. H. Meyer, G. Wegner, *Chem. Mater.* **1998**, *10*, 460; e) H. Cölfen, L. Qi, *Chem. Eur. J.* **2001**, *7*, 106.
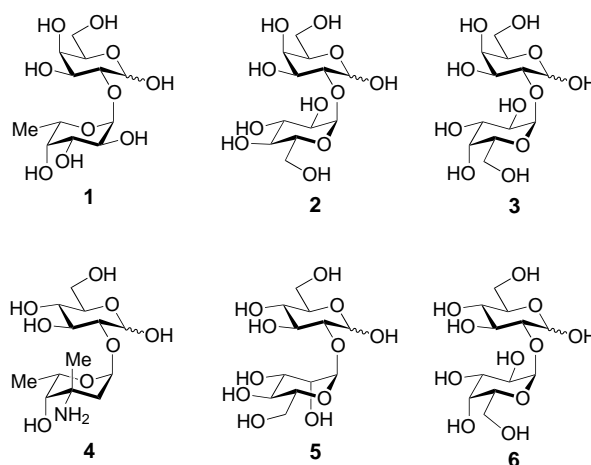
[20] A. P. Chichagov, V. V. Ilyukhin, N. V. Belov, *Sov. Phys. Dokl.* **1966**, *11*, 11.

[21] L. Onsager, *Ann. N. Y. Acad. Sci.* **1949**, *51*, 627.

[22] M. Nikl, P. Bohacek, E. Mihokova, M. Kobayashi, M. Ishii, Y. Usuki, V. Babin, A. Stolovich, S. Zazubovich, M. Bacci, *J. Lumin.* **2000**, *87*, 1136.

[23] L. Qi, H. Cölfen, M. Antonietti, *Nano. Lett.* **2001**, *1*, 61.

[24] A. Peytcheva, M. Antonietti, *Angew. Chem.* **2001**, *113*, 3484; *Angew. Chem. Int. Ed.* **2001**, *40*, 3380.

[25] M. M. Chirilaa, K. T. Stevensa, H. J. Murphyb, N. C. Giles, *J. Phys. Chem. Solids* **2000**, *61*, 675.

[26] K. Polak, M. Nikl, K. Nitsch, M. Kobayashi, M. Ishii, Y. Usuki, O. Jarolimek, *J. Lumin.* **1997**, *72–74*, 781.

[27] Y. Toyozawa, M. Inoue, *J. Phys. Soc. Jpn.* **1966**, *21*, 1663.

[28] M. Springis, V. Tale, I. Tale, *J. Lumin.* **1997**, *72–74*, 784.

[29] M. Nikl, P. Straková, K. Nitsch, V. Petíek, V. Múka, O. Jarolímek, J. Novák, P. Fabeni, *Chem. Phys. Lett.* **1998**, *291*, 300.

## Synthesis of Biologically Potent $\alpha 1 \rightarrow 2$-Linked Disaccharide Derivatives via Regioselective One-Pot Protection – Glycosylation**

Cheng-Chung Wang, Jinq-Chyi Lee, Shun-Yuan Luo, Hsin-Fang Fan, Chin-Ling Pai, Wei-Chieh Yang, Lung-Dai Lu, and Shang-Cheng Hung*

*Dedicated to Professor Chun-Chen Liao*
*on the occasion of his 60th birthday*

$\alpha 1 \rightarrow 2$-Linked disaccharides are key subunits of numerous biologically potent oligosaccharides, antigens, antibiotics, glycoproteins, and glycolipids. For example, the tumor antigen Globo H,[1] ABH blood groups,[2] and human milk oligosaccharides[3] contain $\alpha$-L-Fuc(1→2)D-Gal (**1**) as a common component. $\alpha$-D-Glc(1→2)D-Gal (**2**) is a structural element of glycoproteins isolated from the body wall of leeches.[4] $\alpha$-D-Gal(1→2)D-Gal (**3**) is found as the disaccharide repeating unit of *Streptococcus pneumoniae* type 15 antigen.[5] Vancomycin, a significant glycopeptide antibiotic against grampositive bacteria, has a disaccharide moiety **4**, which consists of $\alpha 1 \rightarrow 2$-linked vancosamine with D-glucopyranose.[6] $\alpha$-D-Man(1→2)D-Glc (**5**) is a typical constituent in the cell membrane of halophilic bacteria.[7] The glycolipids extracted from *Lactobacillus casei* A.T.C.C. 7469 are composed of $\alpha$-D-Gal(1→2)$\alpha$-D-Glc(1→1)-glycerol lipid **6** as the major com-

[*] Dr. S.-C. Hung, C.-C. Wang, S.-Y. Luo, H.-F. Fan, C.-L. Pai
Institute of Chemistry, Academia Sinica
Taipei 115 (Taiwan)
Fax: (+886) 2-2783-1237
E-mail: schung@chem.sinica.edu.tw

J.-C. Lee, W.-C. Yang, L.-D. Lu
Department of Chemistry, National Tsing Hua University
Hsinchu 300 (Taiwan)

Supporting information for this article is available on the WWW under http://www.angewandte.org or from the author.

ponent.[8] Given the importance of these disaccharide motifs with $\alpha 1 \rightarrow 2$ linkages, there is a need to develop a highly selective protection[9] of hexopyranosides to generate a free hydroxy group at C2 for their synthesis. To tackle this problem, we describe herein a highly regioselective benzyl or allyl protection of hexopyranosides to the corresponding 2-hydroxy compounds by means of very mild, acid-catalyzed, reductive etherification of their O-trimethylsilylated derivatives with a variety of aldehydes.[10] Finally, we show their applications in the regioselective one-pot protection – glycosylation to prepare these biologically potent $\alpha 1 \rightarrow 2$-linked disaccharide derivatives.

The one-pot synthesis of the trimethylsilyl ether **8** from methyl $\alpha$-D-glucopyranoside **7** in 74% yield was carried out through a combination of 4,6-O-benzylidenation and 2,3-di-O-silylation. Triethylsilane-reductive O3-etherification of **8** with various aryl and $\alpha,\beta$-unsaturated aldehydes in the presence of trimethylsilyl trifluoromethanesulfonate (TMSOTf) as the catalyst successfully afforded the corresponding 2-hydroxy compounds **9 – 15**. Excellent selectivity and yields were observed in comparison with known methods for the regioselective introduction of acyl or alkyl groups in D-glucopyranosides at O3 (Table 1).[11] Under these acidic conditions, it was observed that the 4,6-O-benzylidene acetal of **8** was not hydrolyzed or opened, and that the double bonds of allyl ethers **14** and **15** were not further reduced. The regiochemistry of **9 – 15** was determined through the $^1$H and $^1$H,$^1$H COSY NMR spectra: H2 was correlated with the proton of the free hydroxy group as well as with H1. The high selectivity is perhaps induced not only by the steric hindrance between the anomeric methoxy group and the 2-OTMS group, but also by the inductive effect of two anomeric oxygen atoms which causes a decrease in the nucleophilicity of O2.

We studied the regioselective etherification in a variety of O-trimethylsilylated pyranosides (Table 2). The highlights include 3-O-benzylation of different protected D-glucopyranosides and $\alpha,\alpha'$-trehalose, and 6-O-benzylation of $\beta$-cyclodextrin as well as of the D-galactopyranosyl derivatives. The 4,6-O-isopropylidene ketal **16**, $\alpha$-allyl ether **18**, and $\beta$-D-thioglucopyranoside **20** were selected to examine the compatibility of substituted groups at the O4, O6, and anomeric positions, and the corresponding 3-OBn compounds **17**, **19**,